Astron. Astrophys. 320, 620–630 (1997)

ASTRONOMY AND ASTROPHYSICS

Yohkoh observations of flares with flat hard X-ray spectra

F. Fárník[1], **H. Hudson**[2], **and T. Watanabe**[3]

[1] Astronomical Institute, 251 65 Ondřejov, Czech Republic
[2] Institute for Astronomy, University of Hawaii, Honolulu, HI 96822, USA*
[3] National Astronomical Observatory, Mitaka, Tokyo 181, Japan

Received 5 June 1996 / Accepted 9 September 1996

Abstract. A series of flares with exceptionally hard spectral indices in the hard X-ray band occurred on 3 October 1993. The non-thermal bremsstrahlung spectra may extend to a few keV in these events, one of which was detectable in the *Yohkoh* Bragg Crystal Spectrometer at 7 keV as well as by the hard X-ray instruments at higher energies. We present *Yohkoh* soft and hard X-ray imaging, spectroscopy and energetics analysis of these events, with the idea that flares with such flat spectra (power-law as hard as 1.98 below 33 keV) might differ appreciably from ordinary flares. The series of events is strongly homologous, with no systematic variations in structure over a period of 3.5 hours except for jet-like ejecta accompanying Type III/V bursts. Unlike other hard events, these flares are large (footpoint separation about $3\,10^4$ km) and therefore well resolved by the *Yohkoh* imaging instruments. The time variations match the Neupert effect. The hard and soft X-ray images also show footpoint brightening and loop filling. The spikes with the flattest spectra have the weakest Neupert-effect signature, but no perceptible time delays between the hard X-ray time profile and the soft X-ray time derivative. These events do not produce superhot emission but are probably microwave-rich. We find no evidence for large-scale magnetic reconnection in the development of these flares. We note two discrepancies between the observations and the existing numerical hydrodynamic models of flare energetics, and suggest that rapid spike events of this type provide good tests of such models.

Key words: Solar flares – X-rays, gamma rays – radio radiation – magnetic fields

1. Introduction

Solar flares exhibit complex phenomenology involving a wide range of physical conditions. We often use simplified pictures of the physics to help to relate the different kinds of observations involved in their study. The *thick-target model* of solar flares and the consequence of the "evaporation" of chromospheric material into the corona represents a well-defined general scenario for flare energetics. In the meantime, the *Yohkoh* observations in particular have provided a great deal of support for general models of solar flares involving *large-scale magnetic reconnection*. These two views of flares (in no way mutually exclusive) must embrace the observed phenomena, including mass motions, particle acceleration, coronal mass ejection, and various radiation signatures. Both of these concepts attract controversy and neither presently has achieved complete approval. In this paper we analyze a series of flares with exceptionally flat hard X-ray spectra, both because they are quite unusual and because this extreme property may reveal more clearly any discrepancies with accepted scenarios for flare development. A preliminary description of the flares we study, with an analysis of the energetics, has already been given elsewhere by Watanabe (1995).

The thick-target model (Brown 1971; Hudson 1972; Syrovatskii & Shmeleva 1972) envisions the primary coronal magnetic energy to be converted by an unknown process predominantly into large numbers of non-thermal electrons. These electrons lose their energy in the lower solar atmosphere and have several effects there: hard X-ray bremsstrahlung, enhanced ionization, and heating. Following this, heated or heating material rises into the corona in a process termed "evaporation" or "ablation". The coronal plasma then emits thermal soft X-ray emission via line and continuum radiations; it drives energy flow back downwards into the lower atmosphere via conduction and radiation. One observational requirement for such a scenario is that the relationship between impulsive (hard X-ray) and gradual (soft X-ray) fluxes follow the Neupert effect (Neupert 1968; Dennis & Zarro 1993), in which the time integral of the impulsive component resembles the time profile of the gradual component. Li and Emslie (1993) have described this theoretically, and Newton et al. (1996) find extremely satisfactory agreement in impulsive flares on the disk, using a better formalism to describe the relationship. Nevertheless the general conclusion that non-thermal electrons carry a major fraction of the total flare energy (Lin & Hudson 1976), implied by the Neupert effect, has proven difficult to establish observationally (e.g. Acton et

* Present address: ISAS, 3-1-1 Yoshinodai, Sagamihara, Kanagawa 229 Japan

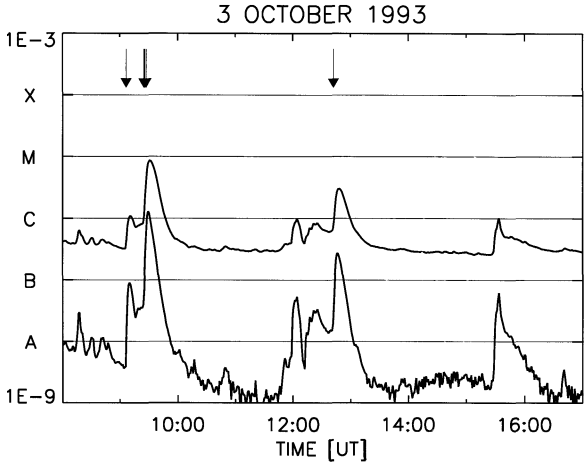

Fig. 1. Time history of soft X-ray flux during the interval of study, from the GOES detectors. The hard X-ray spikes studied are shown with arrows. Note the tendency to similar (homologous) time profiles.

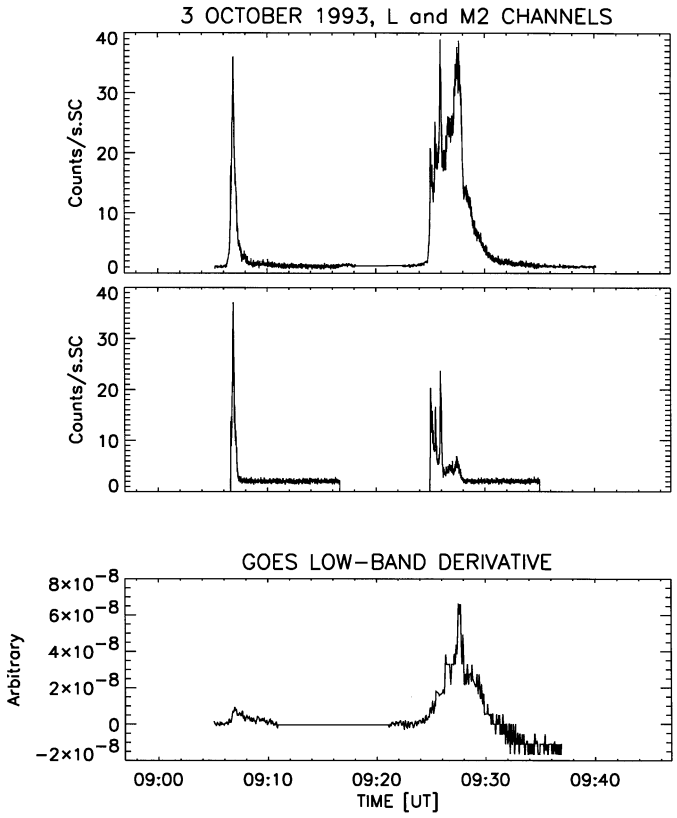

Fig. 2. Comparison of hard X-ray time profile with the time derivative of the soft X-ray time profile, showing the presence of the Neupert effect (Neupert 1968). The upper two plots show the *Yohkoh*/HXT 15-23 keV and 23-33 keV channels. There is a close match in timing, but the initial flat-spectrum event (09:07 UT) corresponds to a relatively small amplitude of the positive soft X-ray derivative compared with the considerably softer event at about 09:28 UT. The time delay between the sharp peaks of the HXT 15-23 keV flux and the time derivative of the GOES flux matches within the 3-sec time resolution of the latter for the initial hard spike (Fig. 3). The early flat-spectrum source also does not show the usual negative swing following the correlated peak.

al. 1982). The bulk energy of the non-thermal electrons is carried at low particle energies in a spectrum normally assumed to be a steep power law. Hard X-ray observations with better spectral resolution have been rare (Lin et al. 1981). Even with the best observations, the estimation of the low-energy cutoff parameter of an assumed power-law primary spectrum is still difficult, because of the integral nature of the bremsstrahlung process (the cross-section $\sigma(h\nu,E)$ varies only as E^{-1}), where $h\nu$ is the photon energy and E the electron energy. Accordingly, given the strength of the Neupert effect correlation, energetics arguments have been used in the past to deduce the low-energy cutoff parameter by simply *assuming* equality of the energies implied by the thermal and the non-thermal X-rays (Tanaka et al. 1984; Watanabe 1995).

Events with comparably flat hard X-ray spectra have been observed previously (e.g. Datlowe et al., 1974; Nitta et al., 1990; Sakao, 1994). The flattest spectra permitted by bremsstrahlung theory would be expected to result from primary electron distribution functions with sharp low-energy cutoffs well above the X-ray observing band (or a monoenergetic spectrum at high energies). Lin and Schwartz (1987) suggested an analog of the auroral electron spectrum, but peaked at higher energies, to account for this behavior. We would like to know if this scenario matches the data.

Magnetic reconnection theory has been applied to solar flares in several ways, but the "opening/closing" scenario is the most highly developed version (Carmichael 1964; Sturrock 1966; Hirayama 1974; Kopp & Pneuman 1976). In this picture magnetic field lines open catastrophically, ejecting material outward. Models of this type have many attractive features, not least of which is their apparent ability to explain coronal mass ejections (Gosling 1990). Other large-scale reconnection theories exist; in all of these theories physical motions of coronal flux systems transport the energy stored in the corona as $B^2/8\pi$ (but see Melrose 1995, for an alternative theoretical discussion).

2. Observations

The data used here principally come from the *Yohkoh* high-energy observations (see the papers in Svestka & Uchida 1991, for full details of the instrumentation). The *Yohkoh* observations have made it possible to learn many things about solar flares (e.g. Hudson & Ryan 1995). The new data include the first imaging observations of hard X-rays above 30 keV as well as extensive soft X-ray imaging and spectroscopy. The flares we study occurred on 3 October 1993 in NOAA active region 7590, near disk center at the time of the observations (N08W02). Table 1 lists the standard NOAA information for this time interval. The first two flares listed occur so close together that they may be thought of as a flare plus a precursor event.

The flare at 15:30 UT turns out to be at a different location within AR 7590, in spite of its similarity in the GOES data (Fig. 1), so we discard it from further discussion in this paper. The flares analyzed in this paper are indicated in the table.

The observations of the first flare of the sequence were incomplete in the *Yohkoh* Soft X-ray Telescope (SXT), and in the

Table 1. NOAA data summary

Date	Begin	Max	End	Class	Hα	AR	Helio		μwave		mwave	
3-OCT-93	09:05	09:09	09:16	C1.0				92	320	220	III	*Yohkoh*
3-OCT-93	09:16	09:30	09:38	C8.6	1B	N08W02	7590	230	200	150	V	*Yohkoh*
3-OCT-93	09:31	09:31	10:05		SB	N12E01	7590					
3-OCT-93	11:57	12:04	12:08	B9.8	SF	N08W01	7590					
3-OCT-93	12:11	12:25	12:37	B8.4	SF	N11E02	7590				III,V	
3-OCT-93	12:40	12:47	12:54	C3.0	SN	N08W03	7590	150	73	79	III,V	*Yohkoh*

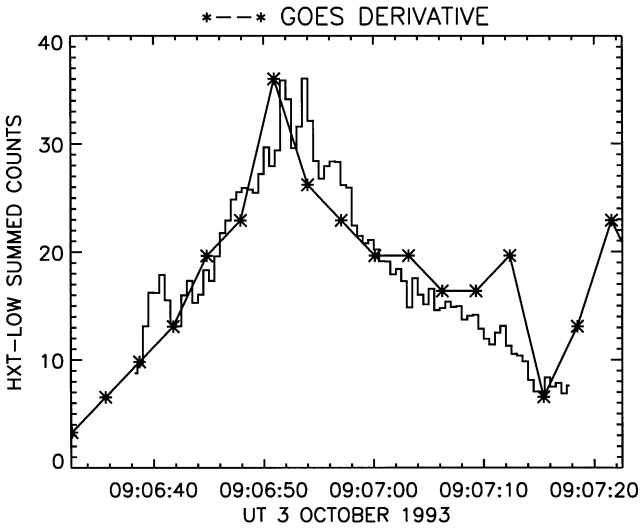

Fig. 3. High-resolution view of the Neupert effect in the first spike: comparison of the HXT 15-23 keV counting rate (plus signs) at 0.5 sec resolution, with the time differences of successive GOES soft channel (2-8 Å) data (asterisks). Within the time resolution of the latter, there is no perceptible advance or delay.

flare at 12:45 UT there was also the problem of a late flare-mode trigger, so that the onset of the initial spike event was not covered by SXT or by the hardest three channels of the Hard X-ray Telescope (HXT). The *Yohkoh* flare flag triggered three times during the interval studied, even for GOES levels below C1, because of the flatness of the spectra. These flares may also have been "microwave-rich," judging from the 15.4 GHz fluxes listed in Table 1.

3. Hard X-ray and soft X-ray timing

We show the time development of the soft X-ray emission in Fig. 1. Two of the three flares in the sequence showed strikingly similar time profiles, with pre-flare and main flare events, and all showed rapid rise times. The hard X-ray time profiles (sums of total HXT counts) of the first events in the sequence (Fig. 2) show the flatness of the hard X-ray spectrum. The index γ approaches the remarkable value of 1.9 (see below), especially in the initial hard spike at about 09:06:50 UT. Here the spectral flux $j(h\nu) = \text{const} \times (h\nu)^{-\gamma}$ ph$(\text{cm}^2 \text{sec keV})^{-1}$. The initial hard X-ray spike at 09:06 notably shows little gradual increase

Table 2. Spectral slope γ and break energy E_b

Time	M1/LOW (γ_L)	HIGH/M2 (γ_H)	E_b [keV]
09:06:45	1.98	3.34	29.0
09:25:00	2.18	3.42	28.5
09:25:50	2.94	4.08	27.0
09:27:15	5.46	-	-
12:42:40	2.42	4.44	26.0

in the soft X-ray channel of HXT, which can detect emission from plasma at temperatures as low as $15\,10^6$ K, although it can be seen in the GOES data (Fig. 1). This means little "super-hot" contribution (Lin & Schwartz 1987). The hard X-ray peak at about 09:26 shows a similar pattern of spikiness and spectral flatness. Three additional spikes occurred in the time range 09:25:00 - 09:26:20, each about twenty seconds in duration and each having flat hard X-ray spectra.

Fig. 2 also shows the relationship between the hard X-ray time profile and the time derivative of the GOES soft X-ray data. This shows general agreement with the Neupert effect: each hard X-ray spike appears to have a counterpart in the soft X-ray derivative, with no discernible delay time (Fig. 3). However the relative amplitudes vary with time and apparently with the hardness of the hard X-ray spectrum. The earliest and hardest spike corresponds to the weakest soft X-ray counterpart. Such an effect had previously been noted by Strong et al. (1985), although not directly in the context of the Neupert effect, in an event that appeared to represent successive excitations within the same loop structure. This and similar observations inspired discussion of electric-field models for non-thermal electron acceleration (Holman 1985; Tsuneta et al. 1985), with some energy supplied via direct heating well as via non-thermal particles (see also Benka & Holman 1994).

4. High-energy continuum

The large-area hard X-ray detectors (BATSE) of the Compton Gamma-Ray Observatory observed parts of these events. From the interval 09:25-09:26 UT, which contains three of the hard spike bursts, we find the normal soft-hard-soft pattern of variation found in ordinary impulsive hard X-ray bursts with softer spectra (Kane 1969). The time profiles of the spike events do

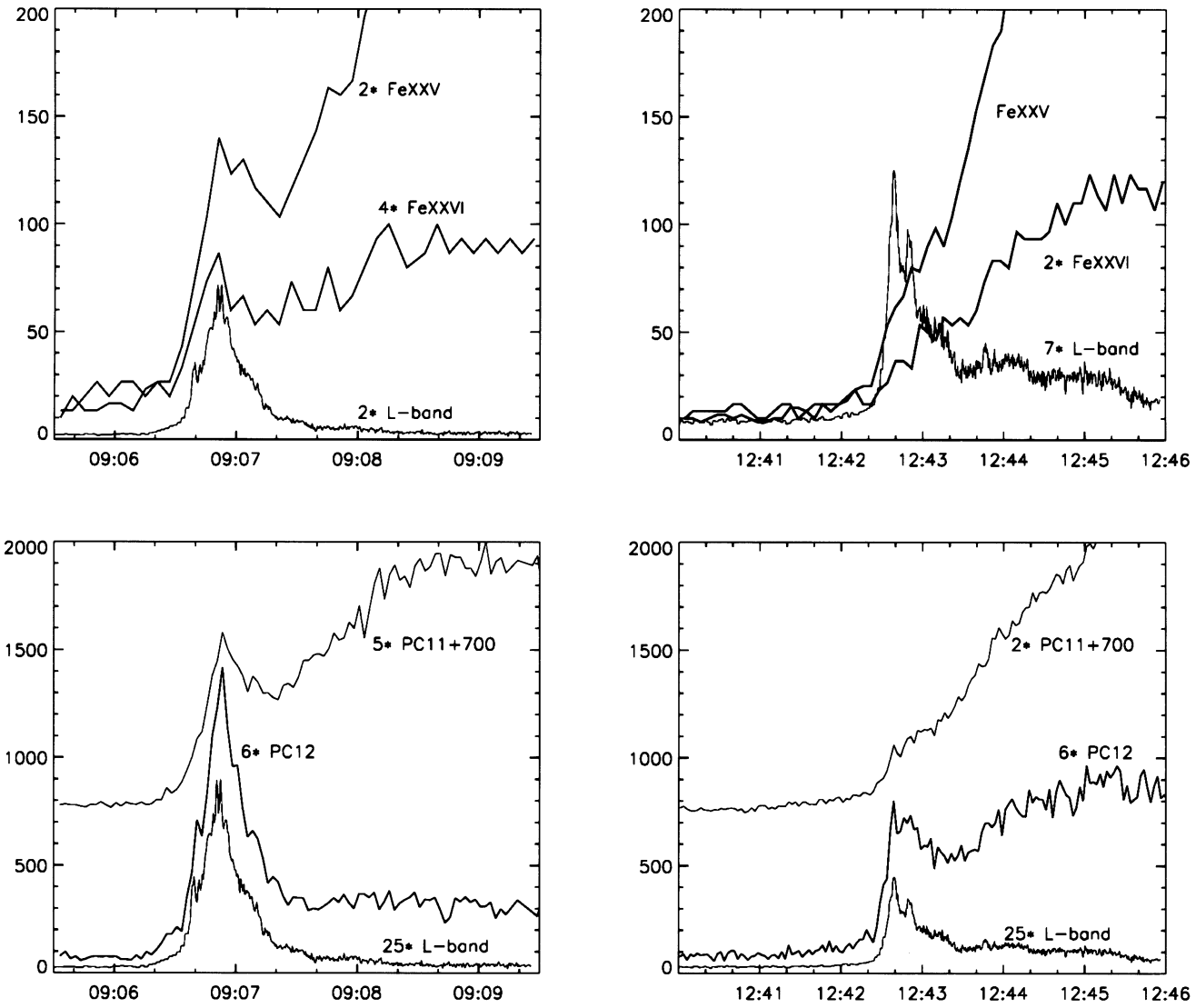

Fig. 4. *Left*:Time profiles of total counts from the *Yohkoh* Bragg Crystal Spectrometer FeXXVI and FeXXV channels (upper), and *Yohkoh* proportional counters (lower) for the earliest burst interval. The spectrometers show clear evidence for the presence of the impulsive non-thermal continuum at 6.7 keV and 7.0 keV. *Right*: Time profiles of total counts from the *Yohkoh* Bragg Crystal Spectrometer FeXXVI and FeXXV channels (upper), and *Yohkoh* proportional counters (lower) for the latest burst interval. The spectrometers show a hint of evidence for the presence of the impulsive hard X-ray continuum at 6.7 keV and 7.0 keV, but it is almost lost in the thermal signal.

not show the remarkable fast-rise-slow-decay pattern of the mm-wave bursts discovered by White et al. (1992). The hard X-ray spectra of the spike events fit broken power laws better than single power laws, but this conclusion is not a strong one because the HXT spectra only have four channels in the energy range 15-93 keV. If the double power-law fit is valid, the break energy (at about 30 keV) may be somewhat lower than in other flares (e.g. Lin et al. 1981) and does not vary significantly with time. Table 2 shows spectral fits from the HXT data.

The transition between the high-energy hard X-ray spectrum (roughly, above 15 keV) and the low-energy continuum contains crucial information about flare energetics and about the nature of particle acceleration. Unfortunately, only the Lin et al. (1981) balloon flight and the scintillation proportional counter on board *Hinotori* (Inoue et al., 1982) have observed with high resolution in this energy range. Tanaka et al. (1984) and Nitta et al. (1990) have analyzed flares using the *Hinotori* observations to obtain broader spectral coverage of the hard continuum. The Nitta et al. (1990) analysis included an event with an extremely flat ($\gamma \sim 1.9$) low-energy continuum resembling those found here (Table 2; 15 sec integrations). We are thus interested in the low-energy points obtained from the *Yohkoh*/BCS spectra (see next section).

5. Low-energy continuum

The spike burst at 09:06:50 generated a detectable continuum signal in the *Yohkoh*/BCS (Bragg Crystal Spectrometer) spectra,

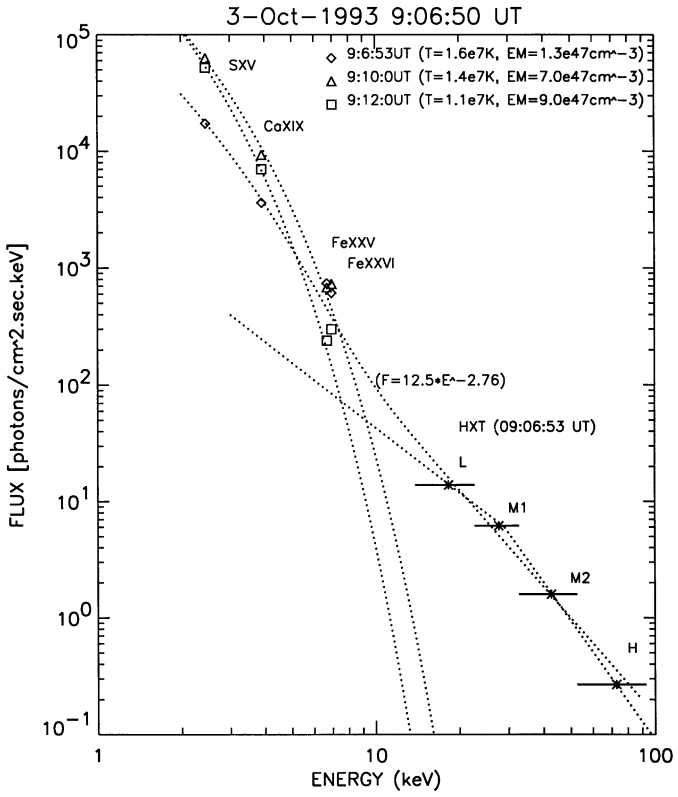

Fig. 5. Continuum spectra inferred from the *Yohkoh*/BCS and *Yohkoh*/HXT total counting rates, during the evolution of the initial flat-spectrum burst. The four HXT channels have been fitted to a broken power law (low-energy index 1.98 $\pm$ 0.04; high-energy index 3.34 $\pm$ 0.03), as well as with a single power law (index 2.76 $\pm$ 0.01). The impulsive source seen in the BCS counters lies somewhat above the extrapolation downwards from the HXT energy range in the two-power-law fit.

which cover narrow spectral ranges at approximately 2.5, 3.9, 6.7, and 7.0 keV, as shown by the time profiles in Fig. 4. These bands cover the He-like line emissions of the SXV, CaXIX, FeXXV, and FeXXVI ions, respectively. An examination of the spectra shows that this excess signal indeed comes from the continuum regions, not the emission lines; both the continua and line-dominated parts in the FeXXV spectra show similar excess during the spike, and the continua do not show those from Germanium-crystal-origin fluorescent photons, which provide a typical shape, reflecting the crystal's apparent solid angles to the instrument detector. The FeXXVI channel is ambiguous in this respect because it normally shows a high continuum level of instrumental origin. The presence of strong continuum in the FeXXV channel is highly unusual, in that the soft X-ray spectrum in this band is normally dominated by the emission lines. Only the two iron channels of BCS show the non-thermal continuum, a result consistent with the higher background rates in the longer-wavelength channels.

We show in Fig. 5 that the low-energy continuum measured in this manner lies near the downward extrapolation of the hard X-ray spectra measured by *Yohkoh*/HXT. The exact shape of the spectrum is difficult to determine from these comparisons, since they are based on different counters with low spectral resolution (one point per BCS detector, since the spectral bandwidth of each detector is small). The significant result, however, is that the non-thermal continuum may extend down to the approximately 7 keV without the further flattening that might be expected from the existence of a low-energy cutoff in the energy distribution of the non-thermal electrons. This extraordinary extension to low energies (see Kahler & Kreplin 1971) was detectable only in the hardest of the spike events.

The significance of the difference between the two fits shown in Fig. 5 is difficult to assess, given the small number of energy channels and the lack of high spectral resolution. The table also shows the break energy, which is similar for all of the entries at about 30 keV. Finally, we note that with HXT it is possible in principle to study spatially-resolved spectra. However we have found that the independent-channel pixon maps (Sect. 6) generated here do not provide sufficiently stable photometry for this purpose. Developments of the imaging software may improve this situation, or "forward method" direct fitting of parametrized models may also generate spatially-resolved spectra (e.g. Sakao 1994, for *Yohkoh* applications of such a technique).

6. Image development

The *Yohkoh* observations have the powerful advantage of showing us the spatial development of the flare structure, on angular scales of a few arc Sect. For the *Yohkoh*/SXT, the images are directly read from a CCD detector with 2.45″ square pixels. For the *Yohkoh*/HXT, a deconvolution procedure is necessary, since the raw data consist essentially of Fourier components of the image. Several techniques for this deconvolution are available, and give similar results for simple structures. We adopt here the "pixon" technique (Piña & Puetter 1993; Puetter & Piña 1994), which improves significantly upon the standard Maximum Entropy Method (Gull & Daniel 1978; see Sakao 1994, for the HXT application), as demonstrated by Metcalf et al. (1996). The soft X-ray and hard X-ray images from *Yohkoh* can be coaligned to a precision on the order of one SXT pixel, peak-to-peak (Masuda 1994).

In the pixon technique as implemented for HXT by Metcalf, the pixons have circular shapes with sizes (as well as brightnesses) as justified by the image statistics. It is possible to set a lower limit on these sizes in order to avoid over-resolution and artifacts that might arise from this. We have accordingly chosen a minimum pixon size of 3 SXT pixels, or about 7.4″. This matches reasonably well with the dimension (FWHM) of the finest elements of the HXT collimator (Kosugi et al. 1991).

We show soft X-ray images with hard X-ray contours overlaid in Fig. 6, selecting times around the peaks of three of the spike events during the first flare (preflare + flare) of the series. The three episodes are strikingly similar. For the first (flattest-spectrum) spike, we unfortunately have no exactly simultaneous soft X-ray images. This gap was caused because the flare onset occurred near the night/day terminator of the *Yohkoh* orbit,

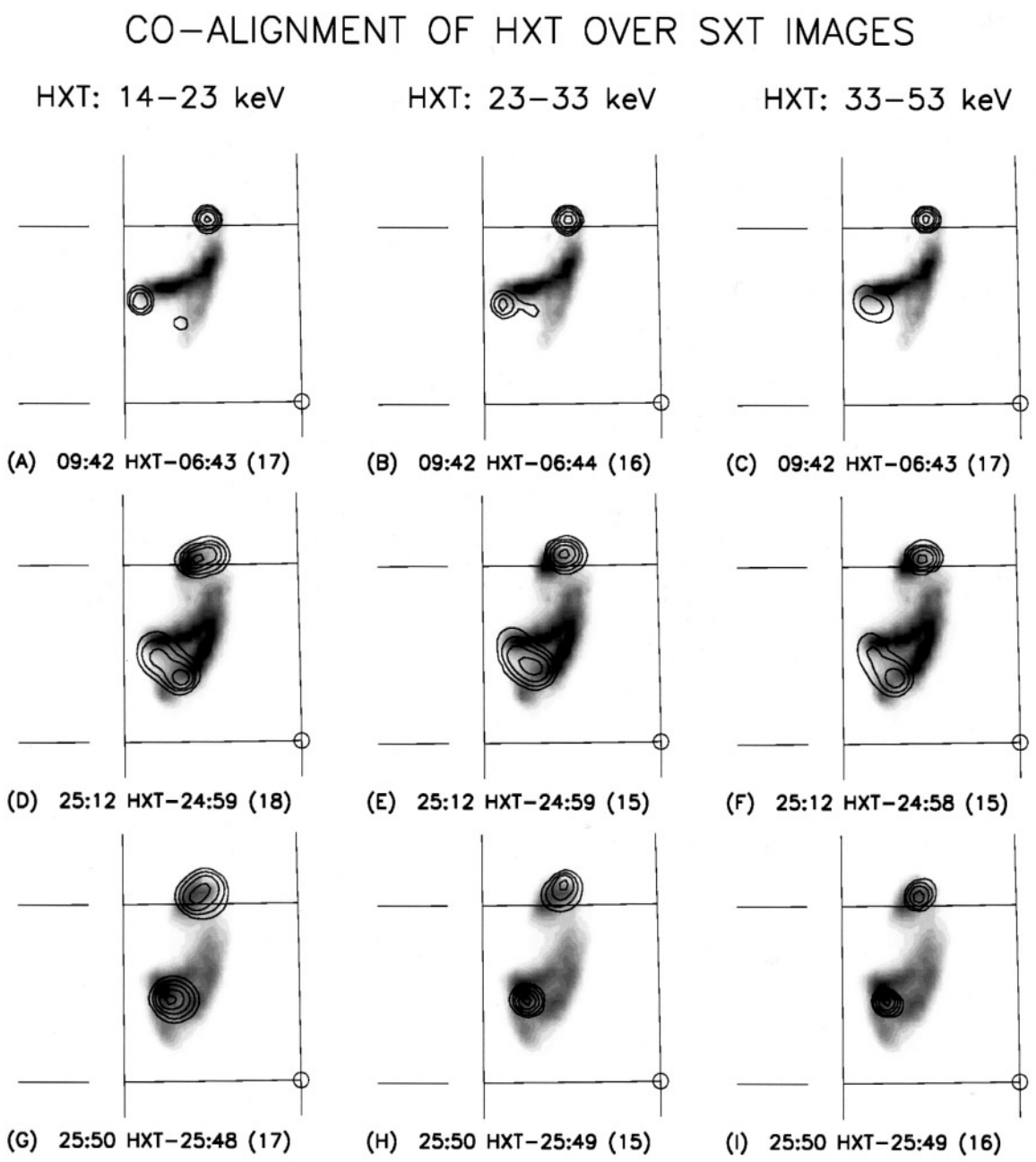

Fig. 6. Hard X-ray images (contours) overlaid on soft X-ray images (gray scale) for three hard X-ray energy ranges, left to right, and for three bursts, top to bottom. For each image the times show the time after 09:00 UT, mm:ss, and the figure in parentheses is the hard X-ray integration time. The circled grid point at lower right in each image indicates heliographic coordinates W05N05, and the contour levels are at 5,10,20,40, and 80%.

while SXT was engaged in "UV flood" preparation of its CCD camera.

These images show strong and well-separated double footpoints in hard X-rays, with connecting arc-like features in soft X-rays. The footpoint separation is on the order of $3\,10^4$ km. The north footpoint in each burst appears to be unresolved by HXT, while the south footpoint is either resolved or consists of multiple bright points (note the tendency of the images in Fig. 6 to break up in the south footpoint region). This pattern strongly suggests the usual morphology of footpoint excitation and loop filling, but there are interesting points of discrepancy: (i) the impulsive footpoint emission expected in soft X-rays (Hudson et al. 1994; McTiernan et al. 1993) is difficult to detect here; (ii) there is a pronounced gap in the soft X-ray loop structure just below the north footpoint; and (iii) there is a striking tendency for the north footpoint to be much more intense, even though it occurs in a stronger field region (see Sect. 7 below).

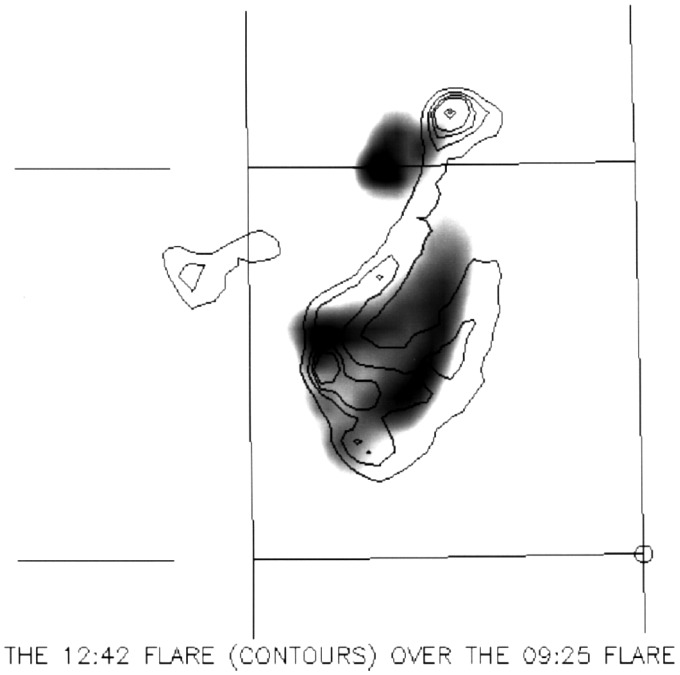

Fig. 7. Overlay of the two flares at 09:25 UT (contours and heliographic coordinates) and 12:42 UT from *Yohkoh*/SXT Be-filter images, with correction for solar rotation. The grid of heliographic coordinates has a small circle at the N05W05 intersection.

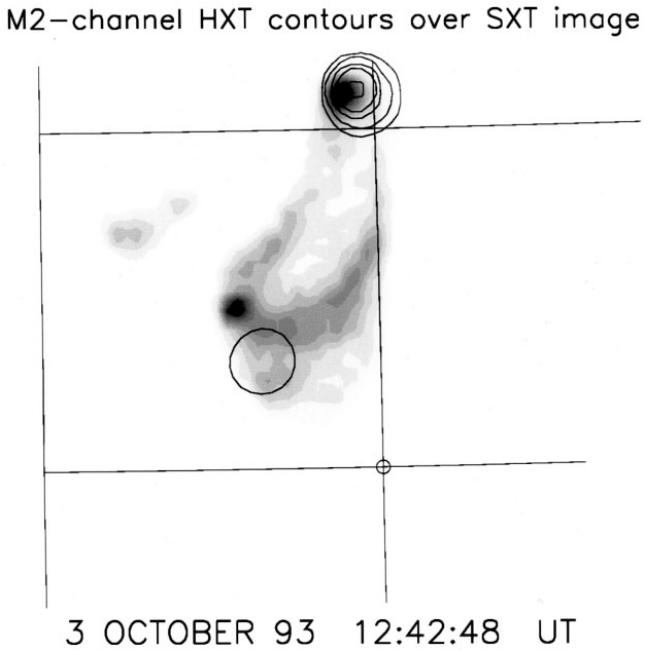

Fig. 8. Overlay of the hard X-ray footpoints as derived from HXT 33-53 keV data (black contours) and the soft X-ray image of the flare at 12:42 UT.

We have searched the soft X-ray images in a pixel-by-pixel manner to try and identify the sites of the hard X-ray emission in the individual spikes. Of the three spikes in the time range 09:25-09:26 UT, we find clear evidence only for the middle event, which can be identified with a compact brightening at the S edge of the N source. The lack of identification of the other sources could result from the relatively poor sampling of SXT (few-msec snapshots approximately 10 sec apart), from obscuration by gradually-varying sources, or from other causes as discussed below. The relative weakness of the soft X-ray response to the flat-spectrum spikes may also play a role.

We find that these flares show examples of fast ejecta readily observable by SXT. These take the form of jets extending to the south and are probably related to the Type III and Type V bursts listed in the NOAA compilations. We do not discuss these further in this paper but note that many other flares also show soft X-ray ejecta (Shibata et al. 1995), as well as Type III bursts, and that the presence of an overdense plasma jet is consistent with the presence of plasma-frequency electromagnetic radiation as required by the emission mechanism of the Type III burst (Kundu et al. 1995).

The flare at 12:45 UT shows strikingly similar image morphology, as illustrated in Fig. 7, in spite of the fact that the flares occurred more than 3 hours apart. Within reasonable limits, the observations are consistent with the idea that approximately the same structure flared repeatedly. This is especially true at the north footpoint, where the image displacements from burst to burst in the first series, after correction for solar rotation, do not exceed the resolution of HXT. Fig. 8 also shows that the hard X-ray footpoints appeared at the same locations as in the previous flare. The separation between the footpoints did not increase. Without being precise in definition, we conclude that from the time series, the spectra, and the image morphology that these flares are strongly homologous.

7. Relationship to magnetic fields

Fig. 9 shows an overlay of the *Yohkoh* X-ray images from the initial flat-spectrum burst with a Kitt Peak magnetogram obtained a few hours after the events (14:30-15:25 UT). Kitt Peak had good data on the previous day as well, and we have estimated a proper-motion correction based upon these two observations. We believe that the overlay is accurate to about two SXT pixels ($\sim$ 5 arcsec).

The north footpoint is more intense (higher surface brightness) in all of the bursts. Since we have limited the pixon sizes in our image construction, this conclusion is conservative. The total fluxes in the two footpoint regions can also be estimated. We have done this both by integrating under the half-maximum contour at each footpoint, and by simply dividing the HXT image into north and south parts between the footpoints. By both methods the ratios of total counts are near unity, north and south, except for the initial burst, and in the 12:42 UT burst, in which there are approximately a 3:1 asymmetries (north stronger).

8. The coronal structure

Judging from the simple hard X-ray images, these events appear to have the classic pattern of footpoint brightening and loop de-

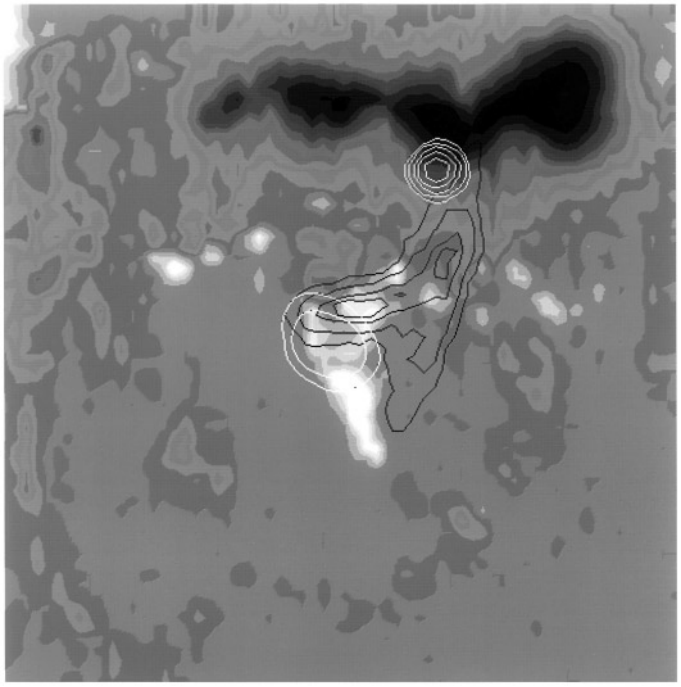

Fig. 9. Overlay of soft X-ray (black contours) and HXT (white contours) on a high-resolution magnetogram from Kitt Peak National Observatory, rebinned to SXT resolution. We estimate the accuracy of the overlay at one SXT pixel (2.46″). The north hard X-ray footpoint lies in a region with more magnetic flux (see text). It continues to have much higher surface brightness throughout the successive bursts.

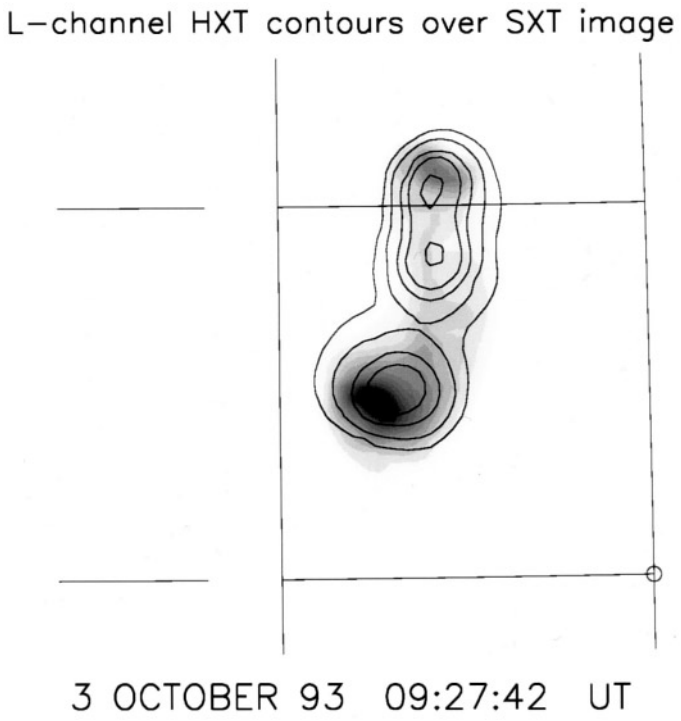

Fig. 10. Image from the HXT 15-23 keV channel (contours) overlaid on an SXT Be-filter image (gray scale). These images are from the "soft" event at 09:27 UT. The hard X-ray contours nicely fill in the region between the footpoints, confirming the existence of a loop structure connecting them. We interpret the HXT image in this case as thermal radiation.

Table 3. North/South footpoint comparison (23-33 keV)

Time UT	North Counts	N Field Mx cm^{-2}	South Counts	S Field Mx cm^{-2}
09:06:50	118	-488	33	+18
09:25:05	39	-358	50	+100
09:25:55	59	-426	62	+46
09:27:30	22	-379	16	+171
12:42:45	22	-969	9	+10

velopment. But the soft X-ray images do not look exactly as they should. Soft X-ray flares often show extremely regular loop structures, and for some purposes (e.g. Aschwanden et al. 1996) they can be approximated as semicircles. Even though our view is from almost directly above the structures (about 6° off the vertical) the soft X-ray loops do not appear as simple arcs. Instead there are concentrations in the north and in the south and a gap in the interconnecting loops near the north footpoint region. These complications could represent independent structures or complicated geometries resulting from magnetic forces. The broad temperature response of the SXT images might also confuse this comparison.

We have attempted to make use of the temperature distributions in the soft X-ray loops to clarify the geometry. Fig. 10 shows an image overlay of the HXT L channel (15-23 keV) in the soft spike phase of the flare at 09:27 UT. The softer hard X-rays clearly extend along the soft X-ray loop structure, but fill in the gap region. This suggests an overall morphology consistent with the simple loop geometry, but leaves some puzzles in the interpretation of the soft X-ray images by themselves. To complete this picture, we have also constructed temperature maps from SXT data (e.g., Fig. 11). These also tend to confirm the simple loop morphology.

Sakao (1994) showed, on the basis of a reasonable sample of *Yohkoh*/HXT events, that the stronger-field footpoint tends to be weaker in hard X-rays, as would be consistent with the mirror force driving the electrons to precipitate preferentially on the weak-field side. We do not confirm this clearly in these events. Certainly the north (stronger-field) footpoint region has the higher surface brightness throughout the whole development. The integrated fluxes are more similar, but in the first (hardest) spike event there appears to be a strong asymmetry in the wrong sense. Fletcher (1996) has investigated this "cornucopia" effect, which may be complicated in such a manner by the details of the field structure and the physics of the particle diffusion.

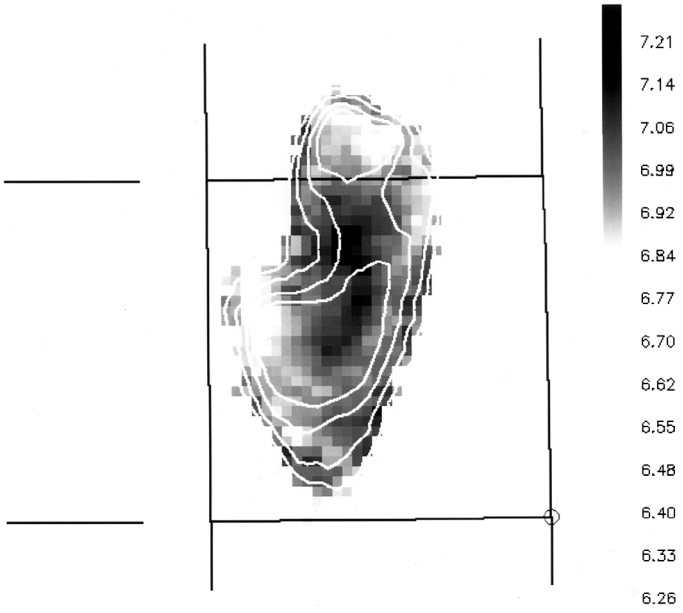

Fig. 11. SXT temperature map, derived from the Be and Al.12 image ratio, with contours of the SXT Be image at 09:27:06 UT. The highest SXT temperatures occur in the central loop region, consistent with the HXT L-channel map shown in Fig. 9.

Table 4. Loop dimensions

Time:	09:07	09:25
Loop Length [cm]		
L1:	$4.6\ 10^{9}$	$4.6\ 10^{9}$
L2:	-	$3.8\ 10^{9}$
Footpoint Area [cm^2]		
A1:	$3.6\ 10^{17}$	$3.6\ 10^{17}$
A2:	-	$3.6\ 10^{17}$
Volume [cm^3]		
V1:	$1.7\ 10^{27}$	$1.7\ 10^{27}$
V2:	-	$1.5\ 10^{27}$

Table 5. Temperature [MK], emission measure [cm^{-3}], and electron density [cm^{-3}]

Time:	09:11:40	09:29	09:32
Temperature			
CaXIX:	10	12	11
SXV:	9	-	-
Emission Measure			
CaXIX:	$1.2\ 10^{48}$	$8.0\ 10^{48}$	$1.0\ 10^{49}$
SXV:	$8.0\ 10^{47}$	-	-
Density			
CaXIX:	$2.7\ 10^{10}$	$5.0\ 10^{10}$	$5.6\ 10^{10}$
CXV:	$2.2\ 10^{10}$	-	-

Table 6. Secondary parameters

Time:	09:07	09:30
Total Number of Electrons, N_e:	$4.2\ 10^{37}$	$1.8\ 10^{38}$
Upflow Velocity, v, [km/s]:	300	180
Upflow Density, n_e, [cm^{-3}]:	$2.0\ 10^{10}$	$6.0\ 10^{10}$
Total Thermal Energy, E_{Th}, [ergs]:	$6.0\ 10^{29}$	$9.0\ 10^{29}$

9. Energetics

We have analyzed the energetics of the first flare event in order to assess the relationship between the non-thermal electrons responsible for the hard X-ray bremsstrahlung, and the soft X-ray sources in the loops. We have done this both for the initial hard spike at 09:07 UT, and for the following hard spike at 09:25 UT. The results are given in Table 4 (observed loop parameters), Tables 5 and 6 (inferred parameters), and Table 7 (non-thermal energy input). In Table 7, total energy inputs are implied by integrating single power-low spectra derived from each channel pairs during hard X-ray spikes. Flat spectra give lower energy input than steeper spectra, if the same cut-off energy is assumed. We find for the first event an energy equality at an assumed cutoff energy of roughly 5 keV, which is consistent with the detection of the non-thermal continuum at the low energies of the BCS counters. The comparison is only semi-quantitative because of the difficulty of the hard X-ray spectral measurements (poor sampling in energy and low resolution). The second event seems to require a higher cutoff of the non-thermal spectrum, which would be consistent with the higher density inferred (Table 5) and the conjecture that an enhanced density can suppress non-thermal particle acceleration in favor of direct heating (Strong et al. 1984; Holman 1984; Tanaka et al. 1984; Tsuneta 1984).

In this energetics analysis, we do not consider the details of the "firm X-ray" band (i.e., the intermediate region, 5-15 keV, between the thermal and non-thermal domains). Nitta et al. (1990) discuss the effects of different interpretations of this region on an energetics analysis. We do not have high-resolution data here, unfortunately.

10. Conclusions

We have described *Yohkoh* and related (GOES and CGRO) observations of a series of solar flares with extremely flat hard X-ray spectra. We find generally that these flares, in spite of the flatness of their hard X-ray spectra, look more or less normal from the point of view of the general loop-filling (Neupert effect) behavior of other flares. Energetically too, this picture seems reasonable. Numerical simulations (Antonucci et al. 1993) predict that the harder electron spectrum should drive less evaporative flow, and that is what we observe in the variability of the Neupert-effect signatures of the different spike events. The simple physical explanation for this is that the more energetic electrons bury themselves in the denser atmospheric layers, where their heating can be suppressed by radiation be-

Table 7. Non-thermal property

Cut-off Energy [keV]	Total Energy Input [ergs] M1/LOW	M2/M1	HIGH/M2
	First Peak at 09:07 UT		
20	$6.6\,10^{28}$	$1.3\,10^{29}$	$3.2\,10^{29}$
10	$1.6\,10^{29}$	$5.6\,10^{29}$	$2.7\,10^{30}$
5	$3.6\,10^{29}$	$2.5\,10^{30}$	$2.3\,10^{31}$
	Second Peak at 09:25 UT		
20	$2.2\,10^{29}$	$4.7\,10^{29}$	$6.5\,10^{29}$
10	$1.2\,10^{30}$	$5.7\,10^{30}$	$8.4\,10^{30}$
5	$7.6\,10^{30}$	$8.5\,10^{31}$	$1.4\,10^{32}$

fore it can drive strong outward flows. One point of discrepancy, however, is that these same simulations predict a delay between the hard X-ray and evaporation signatures, which we do not observe. We also note the mismatch with the Neupert effect after the initial spike, where the usual negative swing of the soft X-ray derivative does not seem to occur. Our feeling is that the models therefore are not consistent with the observations, and we encourage model-builders to examine extreme events of this type to improve their machinery if need be. The models are not sophisticated at the present time, considering the range of physical processes included, and Antonucci et al. state "...single loop flare models based upon energy deposition by an electron beam in the loop atmosphere cannot reproduce the observed soft X-ray time profile...", a consideration that should be compared with the remarkable correlation seen in Fig. 3, for example.

The extension of the non-thermal hard X-ray spectrum to low energies is the principal point of interest in these observations. This has clear significance for flare energetics, because (especially for a softer hard X-ray spectrum) the energy inferred from a low-energy extrapolation of the electron spectrum can become quite large. We note that this event and other flat-spectrum events that have been reported (Datlowe et al., 1974; Nitta et al., 1990; Sakao, 1994) have indices that cluster near 2.0. This result does not seem strictly consistent with the idea that solar-flare electrons have peaked distributions, as found in the auroral zone (e.g. Lin and Schwartz, 1987), but this may be the result of the difficulty of the measurements. A slope significantly steeper than the limit of about 1.4 resulting from the bremsstrahlung cross-section itself might imply the need for a low-energy tail of accelerated electrons, as for example expected from a runaway electron model (Holman, 1985; Tsuneta, 1985).

The events discussed here, with their flat hard X-ray spectra, remind us of the "electron-rich" events discovered by SMM (Rieger & Marschhäuser 1990). In such events, the bremsstrahlung continuum dominates the nuclear line spectrum in the γ-ray line range 1-10 MeV. This implies an unusually powerful electron acceleration relative to the ion component. This identification must remain speculative, however, because our events were not powerful enough for γ-ray observations.

The events also have the characteristic time scales of the "impulse response" flares studied by White et al. (1992) at radio wavelengths. This paper might provide a first look at soft X-ray and hard X-ray images of such events, assuming that we can identify the types. This identification suggests an interesting possibility, which unfortunately must remain at the level of a speculation here. White et al. made VLA images with extremely high resolution, and in their prototype event found that the source dimensions were extremely small. Such a source would not be resolvable by either of the *Yohkoh* telescopes, nor probably by the Kitt Peak magnetograph. This opens the possibility that the main flare event occurred in an undetected (compact) bipolar structure at the north footpoint of the 3 October flares; the larger loops then would be produced by a secondary phase of excitation. This would resemble the flares studied by Kosugi et al. (1994) and Sterling (1994), Hanaoka (1996) and Nitta et al. (1996), in which a compact loop appears to interact at one footpoint with a larger-scale loop. In these events, however, the large-scale loop invariably follow the compact loop in time, whereas our events are simultaneous.

From the accumulated information about these flat-spectrum events, what can we learn about magnetic reconnection? First, we note that we have observed no systematic structural variations, even from flare to flare, except for the jets presumably associated with the Type III/V radio emission. Thus large-scale reconnection seems to be implausible, either in a coronal "opening and closing" context (Carmichael 1964) or in an emerging-flux scenario (Heyvaerts et al. 1977), and the homologous pattern of preflare/flare occurrence would require an improbable ad hoc explanation in an emerging-flux scenario. We see no footpoint motions as would be expected in the latter case. The archive magnetograms show no obvious pattern of flux emergence on these time scales, with most of the observed proper motion in the east-west direction. Accordingly, the simplest explanation for these flares in terms of magnetic reconnection would be that it proceeded internally to the observed flux tube, i.e. in unresolved fibers, and that this energy release drove the ejections that were observed.

Acknowledgements. Yohkoh is a mission of the Institute of Space and Astronautical Sciences, Japan. FF is grateful to the Japan Society for the Promotion of Science for supporting his visit to ISAS. The work of HSH was supported by NASA under contract NAS8-40801. We would like to thank R.C. Canfield and S. Savy for helpful discussions regarding the Neupert Effect, to J. Khan for discussions of reconnection and homology, to T. Sakao, J. Sato and M. Takahashi for their help with the HXT and BCS spectral analysis, and to N. Nitta for an overall critical review. The CGRO/BATSE data were kindly supplied by the BATSE team at MSFC and the Solar Data Analysis Center at GSFC. Finally we thank K. Harvey for providing the magnetogram shown in Fig. 9.

References

Acton, L.W., Canfield, R.C., Gunkler, T.A., Hudson, H.S., Kiplinger, A.L., and Leibacher, J.W. 1982, ApJ, 263, 409

Acton, L.W., Feldman, U., Bruner, M., Doschek, G.A., Hirayama, T., Hudson, H., Lemen, J.R., Ogawara, Y., Strong, K.T., and Tsuneta, S. 1992, PASJ, 44, L71
Antonucci, E., Dodero, M.A., Martin, R., Peres, G., Reale, F., and Serio, S. 1993, ApJ, 413, 786
Aschwanden, M.J., Kosugi, T., Hudson, H.S., Wills, M.J., and Schwartz R.A. 1996, ApJ, to be published
Benka, S.G., and Holman, G.D. 1994, ApJ, 435, 469
Brown, J.C. 1971, Solar Phys., 18, 489
Canfield, R.C., Hudson, H.S., Leka, K.D., Mickey, D.L., Metcalf, T.R., Wuelser, J., Acton, L.W., Strong, K.T., Kosugi, T., and Sakao, T. 1992, PASJ, 44, L111
Carmichael, H. 1964, in AAS–NASA Symposium on the Physics of Solar Flares, NASA SP–50, ed. W.N. Hess, p. 451
Datlowe, D.W., Elcan, M.J., and Hudson, H.S. 1974, Solar Phys. 39, 155
Dennis, B.R., and Zarro, D.M. 1993, Solar Phys., 146, 177
Fletcher, L. 1996, A&Ap 310, 661
Gosling, J.T. 1990, in C.T. Russell, E.R. Priest, and L.C. Lee (eds.), Physics of Magnetic Flux Ropes, (Washington:AGU), p. 343
Gull, S.F., and Daniel, G.J. 1978, Nature, 272, 686
Hanaoka, Y. 1996, Solar Phys., 165, 275
Heyvaerts, J., Priest, J., and Rust, D.M. 1977, Solar Phys., 255, 255
Holman, G. 1985, ApJ, 293, 584
Hudson, H.S. 1972, Solar Phys., 24, 414
Hudson, H.S., and Ryan, J. 1995, ARA&A, 33, 239
Hudson, H.S., Strong, K.T., Dennis, B.R., Zarro, D., Inda, M., Kosugi, T., and Sakao, T. 1994, ApJ, 422, L25
Inoue, H., Koyama, K., Mae, T., Matsuoka, M., Ohashi, T., Tanaka, Y., and Waki, I. 1982, Nuclear Instr. Meth., 196, 69
Kahler, S.W. and Kreplin, R.W. 1971, ApJ, 168, 531
Kane, S.R. 1969, ApJ, 157, L139
Kosugi, T., et al.1994, Proc. of Kofu Symposium, NRO Report No.360, p.127
Kundu, M.R., Raulin, J.P., Nitta, N., Hudson, H.S., Shimojo, J., Shibata, K., and Rault, A. 1995, ApJ, 447, L135
Li, P., and Emslie, A.G. 1993, ApJ, 417, 313
Lin, R.P. 1985, Solar Phys., 100, 537
Lin, R.P., and Hudson, H.S. 1976, Solar Phys., 50, 153
Lin, R.P., and Schwartz, R.A. 1987, ApJ, 312, 462
Mariska, J.T., Emslie, A.G., and Li, P. 1989, ApJ, 341, 1075
Masuda, S. 1994, Hard X-ray sources and the primary energy release site in solar flares, Ph.D. thesis (University of Tokyo)
McTiernan, J., Kane, S.R., Loran, J.M., Lemen, J.R., Acton, L.W., Hara, H., Tsuneta, S., and Kosugi, T. 1993, ApJ, 416, L97
Melrose, D.B. 1995, ApJ, 451, 391
Metcalf, T.R. Hudson, H.S., Kosugi, T., Puetter, R.C., and Piña, R.K. 1996, ApJ, to be published
Neupert, W. 1968, ApJ, 153, L59
Newton, E.K., Emslie, A.G., and Mariska, J.T. 1996, ApJ, 459, 804
Nitta, N., Dennis, B.R., and Kiplinger, A.L. 1990, ApJ, 353, 313
Nitta, N., Yaji, K., and Hudson, H.S. 1996, in preparation
Pallavicini, R., Serio, S., & Vaiana, G.S. 1977, ApJ, 216, 108
Piña, R., and Puetter, R. 1993, PASP, 105, 630
Puetter, R., and Piña, R. 1994, Experimental Astronomy, 3, 293
Rieger, E., and Marschhäuser, H. 1990, Max '91 Workshop No.3, Estes Park, CO, eds. R. Winglee and A. Kiplinger, pp. 68-76
Sakao, T. 1994, Characteristics of solar flare hard X-ray sources as revealed with the Hard X-ray Telescope aboard the *Yohkoh* satellite, Ph.D. thesis (University of Tokyo)
Shibata, K., Masuda, S., Shimojo, M., Hara, H., Yokoyama, T., Tsuneta, S., Kosugi, T., and Ogawara, Y. 1995, ApJ, 451, L83
Sterling, A.C. 1994, Proc. of Kofu Symposium, NRO Report No.360, p. 131
Strong, K.T., Benz, A.O., Dennis, B.R., Poland, A.I., Leibacher, J.W., Mewe, R., Schrijver, J., Simnett, J., Smith, J.B., and Sylwester, J. 1984, Solar Phys., 91, 325
Sturrock, P.A. 1966, Nature, 211, 695
Svestka, Z., and Uchida, Y. 1991, (eds.), Solar Phys., 136
Syrovatskii, S.I. and Shmeleva, O.P. 1972, SvA, 16, 273
Tanaka, K., Watanabe, T., and Nitta, N. 1984, ApJ, 282, 793
Tsuneta, S. 1985, ApJ, 290, 353
Tsuneta, S., Acton, L, Bruner, M., Lemen, J., Brown, W., Caravalho, R., Catura, R., Freeland, S., Jurcevich, B. Morrison, M., Ogawara, Y., Hirayama, T., & Owens, J. 1991, Solar Phys., 136, 37
Watanabe, T. 1995, in Wang, J., Ai, G., Sakurai, T., and Hirayama, T. (eds.) Proc. of the 3rd China-Japan Seminar on Solar Physics, (Beijing: International Academic Publishers), p. 89
White, S.M., Kundu, M.R., Bastian, T.S., Gary, D.E., and Hurford, G.J. 1992, ApJ, 384, 656

This article was processed by the author using Springer-Verlag LaTeX A&A style file *L-AA* version 3.